

Structure and CO₂ budget of Merapi volcano during inter-eruptive periods

Jean-Paul Toutain · Francesco Sortino ·
Jean-Claude Baubron · Patrick Richon · Surono ·
Sri Sumarti · Anthony Nonell

Received: 25 January 2008 / Accepted: 20 January 2009 / Published online: 19 February 2009
© Springer-Verlag 2009

Abstract Soil temperature and gas (CO₂ concentration and flux) have been investigated at Merapi volcano (Indonesia) during two inter-eruptive periods (2002 and 2007). Precise imaging of the summit crater and the spatial pattern of diffuse degassing along a gas traverse on the southern slope are interpreted in terms of summit structure and major caldera organization. The summit area is characterized by decreasing CO₂ concentrations with distance from the 1932 crater rim, down to atmospheric levels at the base of the terminal cone. Similar patterns are measured on any transect down the slopes of the cone. The spatial distribu-

tion of soil gas anomalies suggests that soil degassing is controlled by structures identified as concentric historical caldera rims (1932, 1872, and 1768), which have undergone severe hydrothermal self-sealing processes that dramatically lower the permeability and porosity of soils. Temperature and CO₂ flux measurements in soils near the dome display heterogeneous distributions which are consistent with a fracture network identified by previous geophysical studies. These data support the idea that the summit is made of isolated and mobile blocks, whose boundaries are either sealed by depositional processes or

Editorial responsibility: P. Delmelle

J.-P. Toutain
Université de Toulouse; UPS (OMP); LMTG,
14 Av Edouard Belin,
F-31400 Toulouse, France

J.-P. Toutain
CNRS, LMTG,
F-31400 Toulouse, France

J.-P. Toutain
IRD, LMTG,
F-31400 Toulouse, France

F. Sortino
Istituto Nazionale di Geofisica e Vulcanologia,
Sezione di Palermo,
V. Ugo la Malfa, 153,
90146 Palermo, Italy

J.-C. Baubron
JcbConsulting,
898 route d'Orléans,
F-45640 Sandillon, France

P. Richon
CEA, DIF, Service Radiochimie Chimie Environnement,
F-91297 Arpajon, France

P. Richon
Equipe Géologie des Systèmes Volcaniques, IPGP, UMR-7154,
CNRS,
F-75005 Paris, France

Surono
DVGHM,
Bandung, Indonesia

S. Sumarti
MVO – Merapi Volcanological Observatory,
Yogyakarta, Indonesia

A. Nonell
CEA, CEN Saclay,
F-91198 Gif sur Yvette, France

J.-P. Toutain (✉)
LMTG, Université de Toulouse- CNRS-IRD-OMP,
14 Avenue Edouard Belin,
F-31400 Toulouse, France
e-mail: toutain@lmtg.obs-mip.fr

used as pathways for significant soil degassing. Within this context, self-sealing both prevents long-distance soil degassing and controls heat and volatile transfers near the dome. A rough estimate of the CO₂ output through soils near the dome is 200–230 t day⁻¹, i.e. 50% of the estimated total gas output from the volcano summit during these quiescent periods. On Merapi's southern slope, a 2,500 m long CO₂ traverse shows low-amplitude anomalies that fit well with a recently observed electromagnetic anomaly, consistent with a faulted structure related to an ancient avalanche caldera rim. Sub-surface soil permeability is the key parameter that controls the transfer of heat and volatiles within the volcano, allowing its major tectonic architecture to be revealed by soil gas and soil temperature surveys.

Keywords Volcano degassing · Soil gases · Imaging · CO₂ flux · Ground temperature · Volatile budget · Geochemical imaging and prospecting

Introduction

Degassing at active volcanoes commonly occurs from central craters, active domes and fumarolic fields. It operates also through distal leakage, with large scale transfer of poorly to non-condensable gases (mainly CO₂ with accompanying minor phases such as H₂, He, ²²²Rn, etc.) through soils (Baubron et al. 1990; Allard et al. 1991; Farrar et al. 1995; Williams-Jones et al. 2000; Chiodini et al. 2005). Whilst some less frequently active volcanoes completely lack significant soil degassing (Toutain et al. 2002), high concentrations of CO₂ are commonly measured in volcanic soils at some distance from the craters of other volcanoes. In some instances, CO₂ concentrations up to 100% have been measured in soils of some active volcanoes. High concentrations of He and ²²²Rn also typically occur (Baubron et al. 1990, 1991; Baubron 1996; Baxter et al. 1999; D'Alessandro and Parello 1997). Convective and advective processes are responsible for diffuse degassing and large flux (up to 1,500 t day⁻¹ of hydrothermal CO₂) have been recorded (Chiodini et al. 2001; Salazar et al. 2001; Lewicki et al. 2003). Thus, soil degassing of CO₂ may contribute significantly to total degassing.

Distal degassing is a spatially heterogeneous process, high gas concentrations and fluxes being recorded in high permeability zones such as faults and fractures (Baubron et al. 1991; Chiodini et al. 2001). Soil gas composition, in particular the He/CO₂ ratio, is a powerful tool to characterize contrasted volatile sources (Baubron et al. 1990) or alteration processes (Toutain et al. 2002). Soil gas flux or concentration mapping is also an efficient way to image the distribution of discontinuities, the extent of the fluid

transfer process and the interaction between fluid transfer and the main structural features of volcanoes (faults, fractures, rims, craters).

In this work, we will focus mainly on soil CO₂ and He. Carbon dioxide is the major gas species in dry volcanic fluids and has various sources: (1) the mantle, (2) crustal carbonates or mineral alteration at depth, (3) organic material. In volcanic soil air, CO₂ concentrations may range from atmospheric values up to 100%. Helium has a constant concentration (5.239±0.004 ppm) in the atmosphere as a result of the balance between input from continuous soil degassing and its escape into space. Soil He concentration is usually in equilibrium with atmospheric air with some fluctuations depending on soil rainwater saturation (Toutain et al. 2002). Due to the high diffusion coefficient of He, only deep sources containing uranium and thorium (i.e., the mantle or crustal rocks) can release appreciable amounts of He. Thus, He is a good indicator of deep and early exsolution of volatiles from depressurized magma, and is used as a marker of rising magma. It is also an exceptional marker of gas leakage and crustal discontinuities (Baubron et al. 1991, 2002; Toutain and Baubron 1999).

Dome volcanoes are characterized by a high degree of structural heterogeneity, and therefore should be suitable sites for imaging the distribution of soil degassing. However, to our knowledge, there have been few soil gas studies of active dome volcanoes. Merapi (Central Java, Indonesia) is one of the most active volcanoes in the world. Its activity is characterized by repeated phases of growth and collapse of a viscous andesitic dome (Voight et al. 2000). Passive degassing occurs continuously from the dome and summit fumaroles, with an average SO₂ flux of about 100 T day⁻¹ (Le Cloarec and Gauthier 2003). Whilst the gas and plume chemistry has been well described (Symonds et al. 1987; Allard et al. 1995; Nho et al. 1996; Le Cloarec and Gauthier 2003; Sortino et al. 2006), diffuse degassing at Merapi has never been investigated. The aim of this paper is to examine the general pattern of diffuse degassing at Merapi volcano, and to evaluate the relationship between diffuse degassing and the structural framework of the volcano during inter-eruptive periods.

Ground surface CO₂ flux measurements are an additional way to detect deep gas leakage, and are useful in rocky areas characterized by a very thin soil layer such as those which are found at the summit of Merapi, or along oversteepened slopes, where a probe cannot be inserted to an appropriate depth. On the lower slopes, heterogeneous, thin and sandy soils are common.

In this paper, we make a first estimate of the CO₂ flux emanating from soils of the non erupting portion of an active dome-volcano assuming that the traverses selected describe the complexity of the structure.

Methods

Merapi volcanic and degassing activity

Merapi volcano (Fig. 1a) is a 2,970 m a.s.l. basalt-andesite stratovolcano. It is currently the most active volcano in Indonesia with a quasi continuous extrusion rate of lava averaging $3,000 \text{ m}^3 \text{ day}^{-1}$ over the last century (Voight et al. 2000). Typical eruptions of Merapi are due to gravitational collapse of over steepened lava domes producing “Merapi-type” nuées ardentes (Voight et al. 2000). Large displacements are observed in the summit area before and during episodes of unrest (Beauducel et al. 2006), reflecting magma dynamics within a highly fractured crater and stress acting upon the rocks of the volcano's feeder system. Merapi's main magma reservoir could be either a 2.6 km^3 magma chamber (Ratdomopurbo 1995), or a system of associated magma pockets (Commer et al. 2006) at about 1.5 km depth.

The summit area of Merapi can be described as a cone with a 600 m diameter base and 300 m height. The southern part consists of a degassing crater which also hosts a growing dome. The dome represents about half of the total volume of the summit, and is inaccessible due to

topography. The northern area displays no magmatic activity and little evidence of degassing except for two fumarole fields (Woro and Gendol, Fig. 1b), and steam condensation along faults.

Merapi is a moderate gas emitter with an average SO_2 flux of about $100\text{--}400 \text{ T day}^{-1}$ (Symonds et al. 1987; Nho et al. 1996). Fumarolic temperatures, as high as 910°C in 2000 (Sortino et al., 2006), are strongly influenced by tropical rainfall (Richter et al. 2004). The summit region is mainly composed of imbricate lava domes, crater rims and pyroclastic deposits, locally highly altered. Soil temperature in this zone, as well as on the upper ESE slope of the crater, can reach more than 60°C (Friedel et al. 2004), thus outlining diffuse degassing.

Tropical rainfall at Merapi is $2,000\text{--}4,500 \text{ mm year}^{-1}$, with distinct rainy and dry seasons (October–March and April–September, respectively). Showers higher than 100 mm day^{-1} are often observed.

Summit and lower flank main structures

The summit area of Merapi is composed of crater rims and lava domes resulting from a complex eruptive history (Camus et al. 2000; Voight et al. 2000). Over time, the

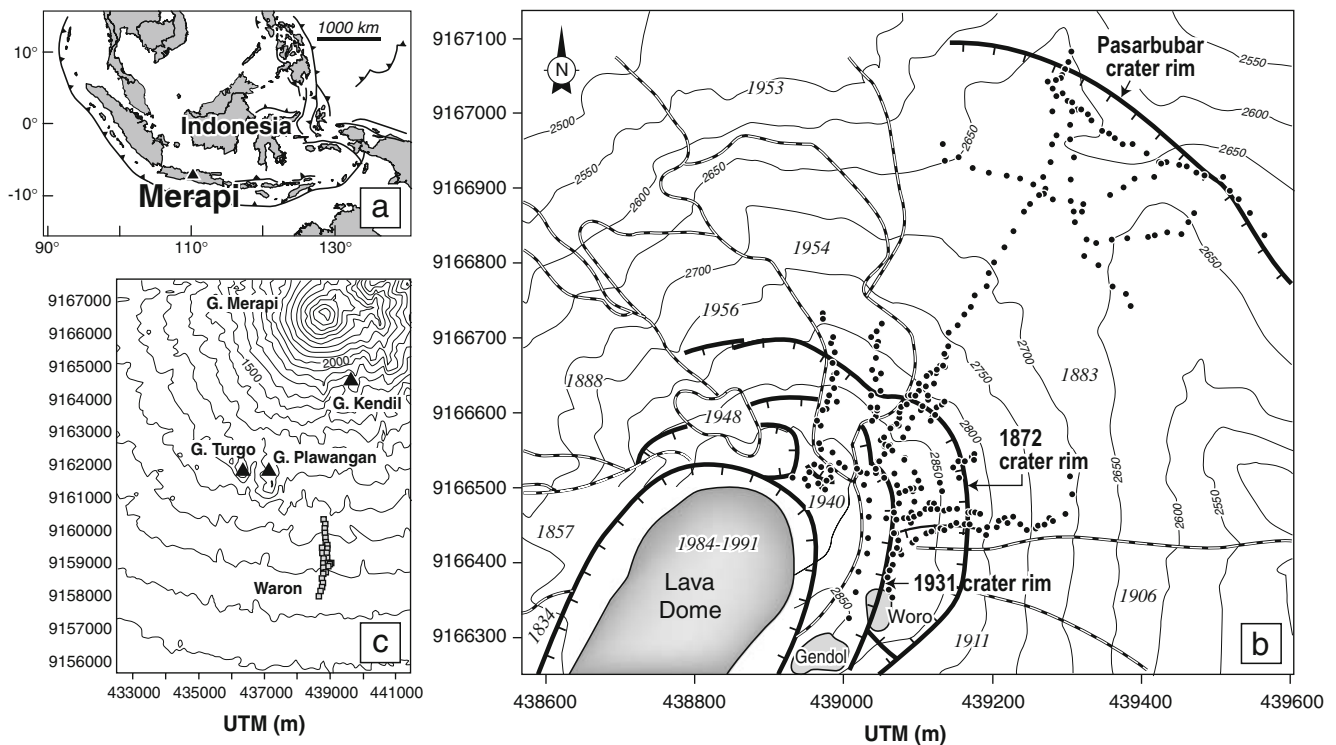


Fig. 1 a Location of Merapi volcano in the Indonesian volcanic arc, b map of the Merapi summit from Camus et al. (2000). The main lava flows, domes and crater rims are indicated. Woro and Gendol are the two main fumarolic fields. Routes are drawn through *full cycles*

indicating sampling point locations, and c location of the traverse used to find the avalanche caldera major fault (Kalscheuer et al. 2007). Coordinates in UTM (m)

successive summit craters and breaches have been partly or completely filled, subsequent eruptions or dome collapses creating new depressions with differing morphologies (Young et al. 2005). Three main structures can be identified (Fig. 1b):

- The “Pasarbubar” crater rim, approximately 2,680 m a.s.l., 700 m wide, inherited from the recent Merapi period and enlarged during the 1768 eruption, which totally destroyed the dome.
- The “Mesjidlanana” crater rim, approximately 2,840 m a.s.l., about 600 m wide and 500 m deep, formed during the powerful 1872 eruption. All domes extruded from 1872 until now are located within this crater.
- The horse-shoe-shaped summit crater (“Senowo crater”), approximately 2,880 m a.s.l., 850×400 m, 250 m deep, which results from the 1930–1932 eruption.

Aside from the active dome, two fumarolic fields allow the degassing of magmatic fluids: Gendol, which occupies the bottom of the 1932 crater, close to the pre-2006 dome, and Woro on the rim of this crater. An active fracture network at the summit is indicated by kinematic GPS measurements and confirmed by Bouguer anomaly mapping, the main directions being about N20°, N80° and N110° (Gunawan 2005; Beauducel et al. 2006).

Since being first mooted by Van Bemmelen (1949), there is growing evidence for a large hyperbolic structure (Bahar 1984; Berthommier 1990; Camus et al. 2000). This huge structure corresponds to the avalanche caldera rim (Camus et al. 2000), which may be related to a still-active hydrothermal convective cell linked with deep levels of the volcanic pile. Recently, electromagnetic evidence for such a structure was obtained near an altitude of 825 m on the southern slope of the volcano, south of Gunung Turgo and Gunung Plawangan (Kalscheuer et al. 2007).

Soil gas concentration mapping and $\delta^{13}\text{C}$ isotopes

Carbon dioxide and He concentrations were measured along traverses intersecting the main structural features of the volcanic pile. In September 2002, during a dry period, we performed 17 soil gas traverses to map CO_2 degassing at Merapi volcano. Helium measurements were performed at selected sites. Three hundred and three CO_2 and 71 He measurements were obtained. Gases were pumped from soils at a rate of 0.2–0.5 L min^{-1} through a stainless steel probe. The sampling depth was 0.6–0.8 m where possible, but sometimes less due to lithologic heterogeneities. Carbon dioxide was determined in the field with a IR-spectrometer (LFG20 - Geogas, UK or a PCO2Plus—GasData, UK), with accuracies of $\pm 0.5\%$, 3% and 5% for concentration ranges of 0–10%, 10–50% and 50–100%, respectively. Soil gas was stored in 1 L teflon bags and

analysed the same day using a specific mass spectrometer (100 HDS-Géo, Alcatel -F) for He concentration at selected sites. Accuracy of measurements is 0.2%, allowing for the detection of very low (down to 5 ppb) anomalies with respect to the typical atmospheric value (Baubron et al. 2002; Toutain et al. 2002). All soil CO_2 and He concentration values were normalized to atmospheric air for local pressure equilibrium, and they were also periodically verified using gas standards. Sampling points were geo-referenced using handheld-GPS measurements (Etrex Garmin, 1 to 10 m accuracy).

Seventeen traverses, ranging in length from 40 to 420 m, were performed in September 2002 (Fig. 1b). They were located in accessible areas that tentatively cross cut the main structural features of the Northern part of the summit cone. However, the sampling site distribution was limited by the rough conditions of the oversteepened slopes. Several areas were investigated: the summit zone, mainly along the 1932 crater rim, radial discontinuities between lava flows and domes, the bulk summit crater through a 420 m-long radial transect, and down slope, the Pasarbubar crater rim area. Four traverses explored the crater slopes from the summit. Two of them follow the main footpath already used for self-potential profiling (Aubert et al. 2000) whereas two others explore the upper slopes northward and eastward, respectively. Two traverses explored the summit area. One of them, NS trending within the Kawahmati depression, ended near Gendol crater, whereas the other explored the 1932 crater rim up to Woro crater. Lastly, two traverses were located down slope on the floor of the 700 m-wide “Pasarbubar” crater.

An interpolated contour map of CO_2 concentrations was derived using an ordinary kriging method (Surfer software), which interpolates concentration values as weighted linear combinations of neighbouring observations.

A north–south traverse on the lower slopes of the volcano was surveyed during the fall of 2007, with a 10 m sampling interval (198 sample sites), from an altitude of 1,000 m down to an altitude of 700 m. Both CO_2 concentration and flux were measured with the addition of He and Rn determinations at specific sites where an electromagnetic anomaly occurred (Kalscheuer et al. 2007). Radon was measured by alpha counting of 125 cm^3 ZnS scintillation bottles with a 600 s integration time (Baubron et al. 1990, 2002). Measurement reproducibility is better than 10%. $\delta^{13}\text{C}$ measurements of both high-temperature fumarolic gas and low-temperature soil gases were performed after collecting the gas phase in two evacuated glass vials. Analyses were carried out using a Finnigan Delta Plus mass spectrometer and the results are given in (δ) notation as per mil (‰) variations relative to the PDB standard with an accuracy of $\pm 0.15\%$.

Soil gas flux traverses

Two hundred and twenty CO₂ flux measurements were obtained by using accumulation of soil gas for about 1 min, in a 1 L, 0.007854 m² chamber. Carbon dioxide concentrations in the chamber were measured every 5 s with an IR spectrometer (EGM4—PP Systems, USA). Flows were calculated from recorded raw data, using the theoretical increasing function of gas concentration with time for advective fluxes (Pinault and Baubron 1996; Welles et al. 2001; Baubron et al. 2004). This approach provides values of both flux and gas concentration entering the accumulation chamber. Uncertainties on individual measurements are lower than 2%, which is much better than the uncertainty due to field heterogeneity. Associated ground temperatures were measured using a K thermocouple inserted to 0.1 m depth.

Results

Summit area: structure from soil gas compositions

Carbon dioxide and He range from 0.04% to 46.4% and from 4.57 to 11.97 ppm, respectively. The highest concentrations of CO₂ and He are typical of hydrothermal/magmatic environments (Baubron et al. 1991; Allard et al. 1998). Low CO₂ contents may be related to altitude-dependent production of biogenic C from plant respiration, bacterial production and decomposition of organic material (Williams-Jones et al. 2000).

At elevations above 2,600 m, the areas investigated lack vegetation, therefore little to no biogenic-derived CO₂ contribution would be expected. This is supported by results from $\delta^{13}\text{C}\text{-CO}_2$ analyses of nine soil gas samples collected in 2001 ($-3.9\pm 0.4\%$ vs PDB), which showed values almost identical to the $\delta^{13}\text{C}\text{-CO}_2$ of the fumarolic gases collected in 2001 and 2007 (-3.9% and -4.3% respectively).

Four populations of soil CO₂ concentrations are associated with variations in soil temperature and moisture from uprising steam and differing He concentrations (Fig. 2):

- Population I (154 samples with CO₂ ranging from 0.03% to 0.05%) are pure-air samples.
- Population II (68 samples with CO₂ ranging from 0.05% to 1%) represents local soil with atmospheric air contaminated by a minor volcanic gas contribution and/or a limited biogenic contribution. Both populations I and II exhibit only atmospheric air He concentrations.
- Population III (51 samples, CO₂ ranging from 1% to 10%) represents sites with a significant contribution of volcanic gases from depth, feeding a hydrothermal cell

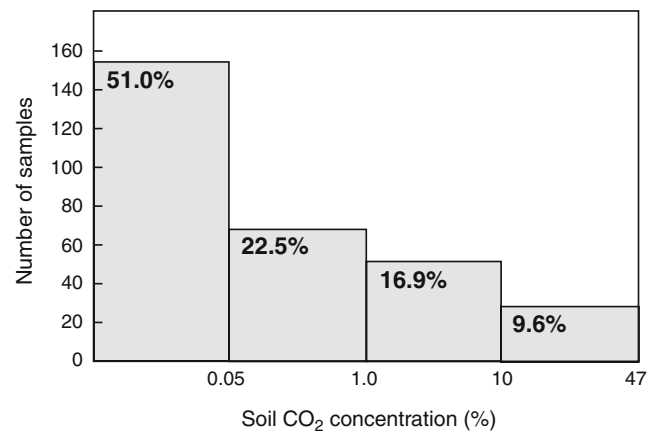


Fig. 2 Statistical distribution by classes of soil CO₂ concentrations measured at the summit of Merapi. The limits of the classes of distribution are shown at the upper left of each box

whose top remains below ground surface, as seen from the lack of steam condensation at these points. At these sites, He concentrations are significantly higher than atmospheric air, but remain lower than 6.0 ppm. This range of helium concentration indicates deep gas leakage with subsequent dilution by atmospheric air but without any evidence of surface degassing.

- Population IV (29 samples, CO₂ higher than 10%) exhibits He anomalies, either up to 12 ppm or below air concentration, the latter due to gas phase separation processes in the hydrothermal cell. These sites correspond to outcropping hydrothermal cells, with weak steam emissions associated with frequent sulphur deposits. Atmospheric air mixing with deep gas is much lower within this population.

Figure 3 is a virtual profile drawn by using the three most representative transects over the whole area, from the summit fumarolic field to the summit crater rim and then down to the Pasarbubar flat crater. It illustrates the similar patterns of CO₂ and He concentrations as observed on many other volcanoes, suggesting a common source for both components. The profile shows a large spatial heterogeneity of gas concentrations and highlights areas with very high concentration gradients. The highest gradient was detected on the eastern slope, with a dramatic transition from concentrations as high as 10% to atmospheric values (360 ppm) within about 30 m. A contour map of CO₂ concentrations measured on the Merapi summit is shown in Fig. 4. In order to use kriging in a rigorous manner, such maps are usually based on uniformly distributed points. The marked roughness and steepness of Merapi's summit area, however, did not allow a uniform distribution of sampling sites. The derived interpolated map should therefore be considered as a rough preliminary

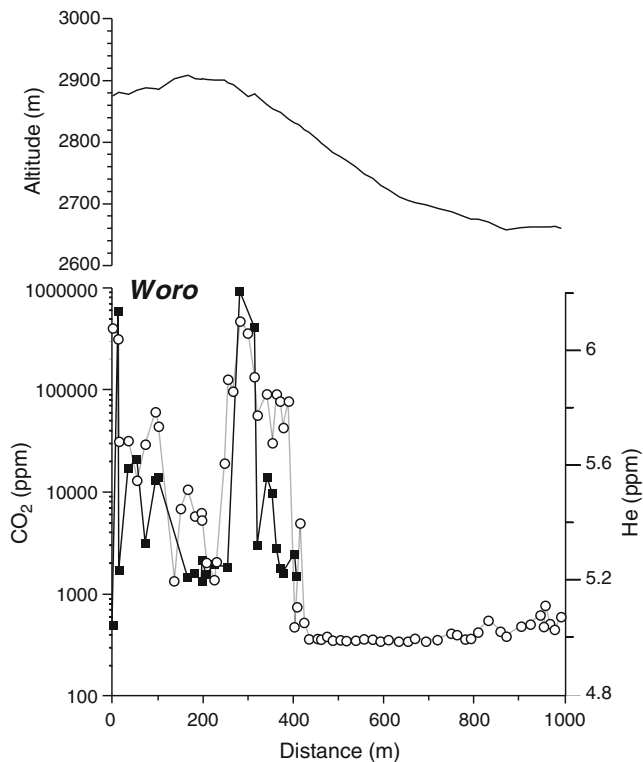


Fig. 3 Virtual profile obtained by plotting together the three most representative traverses of soil CO₂ and He concentrations measured over the whole area, from the summit fumarolic field to the crater rim and then down to the Pasarbubar flat crater. The average sampling step is 10 m. Soil CO₂ data are shown as *open circles*, He data are shown as *solid squares*. GPS-measured altitudes are displayed above the geochemical profiles

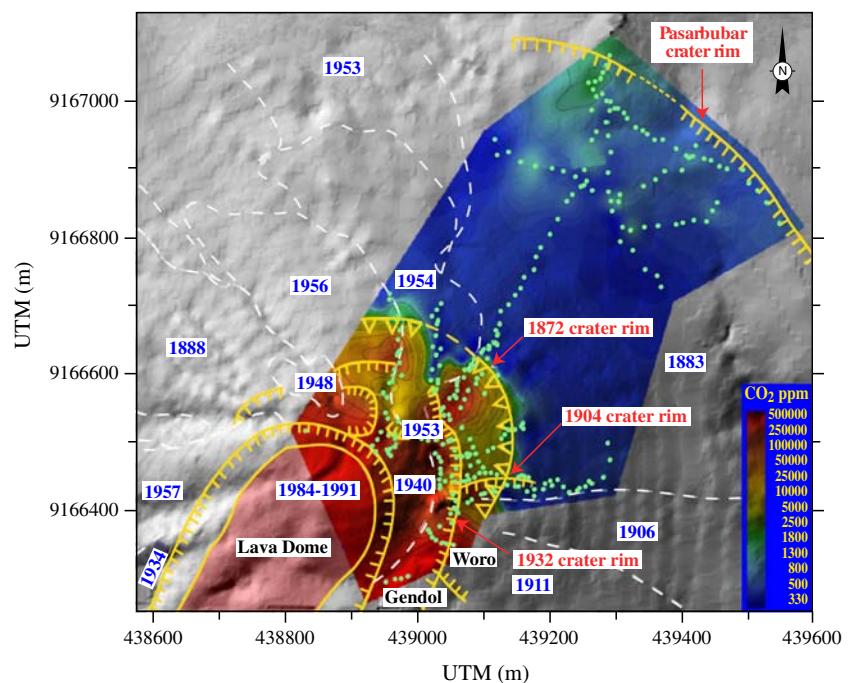
image of the degassing pattern through soils of the inactive northern part of the summit cone. Figure 4 shows that CO₂ concentrations strongly decrease from the summit area down to the Pasarbubar crater rim. Both homogeneous domains and interfaces can be outlined, these latter being potentially related to crater rims.

Both the Pasarbubar bottom crater area and the lower part of the summit cone (zone I), up to altitude about 2,820 m, displayed soil air with atmospheric CO₂ values. Some slightly higher concentrations (up to 0.1%) were observed in the lower area: these values are likely to be due to additional biogenic CO₂ as they coincide with the first signs of sparse vegetation. It is noteworthy that the cliff, forming the Pasarbubar crater rim, does not display any significant CO₂ leakage, unlike many major volcano-tectonic structures.

Zone II is a concentric area westward and up slope of Zone I. It displays CO₂ concentrations up to 10%. Whilst concentrations of biogenic CO₂ up to 5% can be measured in the soil of tropical volcanoes, such values would not be expected here as the area lacks any vegetation. The boundary between Zones I and II matches well with the 1872 “Mesjidanlana” crater rim, in spite of a NE–SW elongated area which displays higher concentrations (up to about 10%). A high temperature spot occurs in the southern part of Zone II, close to the intersecting 1904 crater rim.

Zone III, with CO₂ concentrations up to 46%, is located up slope of zone II, close to the dome and fumarolic fields. The boundary between zone II and III matches the 1932 crater rim eastward of the summit dome. Moist or steaming ground is frequently encountered in this area, suggesting a

Fig. 4 Contour map of soil CO₂ interpolated concentrations measured on the flanks of Merapi volcano. Linear kriging method with Surfer software was used to interpolate data from sampling sites



convective hydrothermal cell close to the surface. Altered ash and sulphur deposits are often present at such sites. The SW transition from zone II to III is less pronounced, and corresponds to the intersection between the NW edge of the 1932 crater rim and the circular truncated buried crater of the 1953 eruption described by Camus et al. 2000 (Fig. 1). Low CO₂ concentrations were measured in the transition zone, indicating only a weak contribution of deep volcanic gas, probably resulting from mixing with atmosphere. Similar observations have been made at the summit of other active volcanoes (Baubron et al. 1991; Pinault and Baubron 1996; Giammanco et al. 1998; Hernandez et al. 2001). Nevertheless, low-CO₂ areas could produce relatively high CO₂ fluxes despite low concentrations, since some of the sites had fluxes of up to 400 g m⁻² day⁻¹ (see “Discussion”), although the CO₂ concentrations were only a hundred parts per million above those of atmospheric air. These areas are mainly found on the upper parts of the slopes, probably as the result of combined wind-driven pressure on the flank of the volcano and the heat released from the whole summit, both resulting in a powerful Venturi effect, sucking atmospheric air deep inside the volcanic pile.

Summit area: soil CO₂ flux and temperature distribution

Fifty measurements of CO₂ flux and ground temperature at 10 cm depth have been performed in the summit area of Merapi (Fig. 5). This zone is characterized by surface fractures, either observed or inferred from ground deformation measurements during recent episodes of unrest

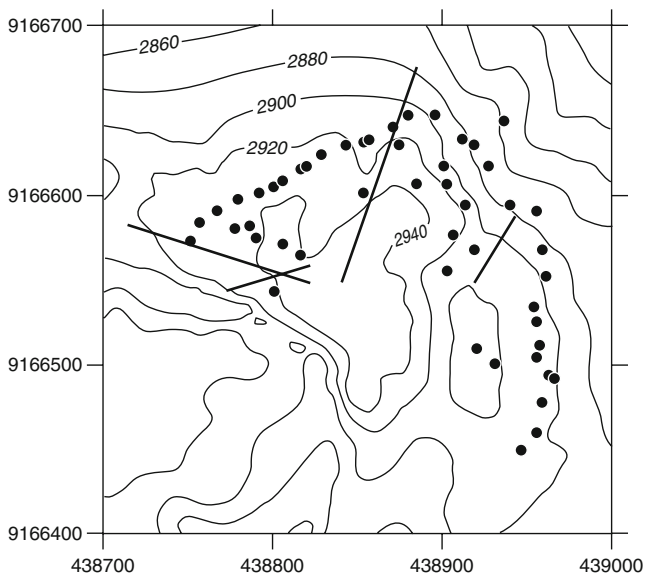


Fig. 5 Digital map of Merapi summit area (Beauducel, pers. comm) showing site locations where measurements of soil CO₂ efflux and ground temperatures were carried out. The main fractures described by Beauducel et al. (2006) are displayed with *black straight lines*

(Beauducel et al. 2006). These fractures are interpreted as mechanical discontinuities resulting from the motion of isolated mobile blocks. Soil temperature (Fig. 6a and c) ranges between 18°C and 80°C, testifying to a large thermal exhaust from the whole summit. If we consider the entire set of soil CO₂ flux and temperature measurements, no clear correlation is observed between the two parameters (Fig. 6a). In detail, however, two distinct populations of data can be identified on this plot, a first representing most of the surveyed area, with CO₂ fluxes lower than 750 g m⁻² day⁻¹ and a second, corresponding to points measured near faulted zones with crushed or altered rocks, characterized by flux values higher than 1,200 g m⁻² day⁻¹. At these locations soil usually appears moist and associated with sulphur deposits. However, similar surface features without any CO₂ flux or any significant temperature anomaly are also encountered close to these sites, suggesting that self-sealing operates gradually and leads to a drastic decrease in soil permeability within a few meters. The feature is consistent with previous unpublished results obtained at volcano summits (for instance Etna or Irazu) where relatively high soil CO₂ flows are measured with only very weak CO₂ concentration anomalies, at the ground surface. For Merapi, the emanating soil CO₂ concentration at the ground surface (i.e. the concentration of the gas entering the accumulation chamber, given by the asymptote of the fitting of concentration relatively to time) reaches only 5,000 ppm above atmospheric air concentration, with different relationships with calculated flux (Fig. 7). A huge inflow of atmospheric air inside the terminal cone, from both wind pressure and thermal draft, can explain this observation (Pinault and Baubron 1996). Even if our data set is rather limited, these features indicate that block boundaries are characterized either by high flows with related temperature anomalies, or most often by no flow zones, with or without soil temperature anomalies, probably as the result of the self-sealing process mentioned earlier. Thus, we can consider blocks as almost homogeneous degassing surfaces, and blocks boundaries as peculiar areas with possibly high flows.

A rough budget of soil degassing through the non-erupting portion of the summit cone during inter-eruptive periods can be calculated using the 2007 measurements. We assume (1) a geometry of half a cone with a 600 m base radius and 300 m height and (2) CO₂ flux values of 240 g m⁻² day⁻¹ for 90% of the surface and 1,480 g m⁻² day⁻¹ for the remaining 10%, in accordance with the data set. This latter value is assigned to block interfaces associated with steaming ground where noticeable heat anomalies and high CO₂ fluxes were measured. From this calculation, a total of about 200–230 T day⁻¹ of carbon dioxide is released from this part of Merapi's summit area, 50–60% from blocks and 40–50% from block boundaries. The contribution of

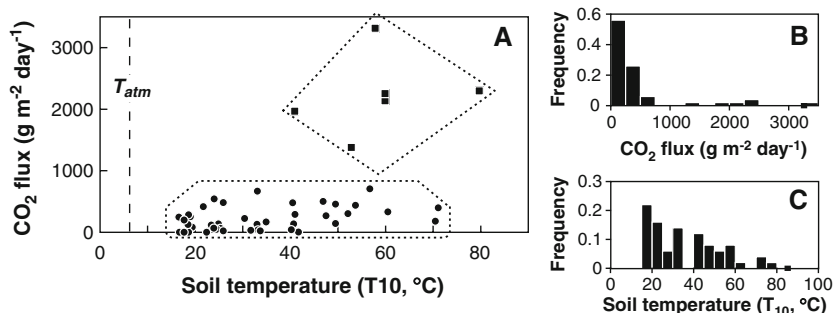


Fig. 6 a Relationship observed at Merapi summit between soil temperature (measured at 10 cm depth) and CO₂ flux emanating from ground surface. b Frequency distribution of CO₂ flux (g m⁻²) at

ground surface. c Frequency distribution of soil temperature (°C, measured at 10 cm depth)

the Woro high temperature fumarolic field cannot be considered in this budget since hot gases are absorbed within the bulk convective plume released by the dome. Soil CO₂ emission from the inaccessible southern half of the cone is probably also incorporated into the summit plume as a result of the steep topography and the immediate vicinity of the active dome.

Southern flank: soil gas anomalies related to major flank collapse-related structure

Using electromagnetic profiles, Kalscheuer et al. (2007) postulated the existence of a major faulted structure below the southern flank that could be an ancient avalanche caldera rim connected to a deep hydrothermal reservoir. A north to south 2,500 m long traverse of 208 sampling sites (Fig. 1c) was carried out at “Waron” for soil CO₂ measurements, along Kalscheuer et al. (2007) profile. Both soil CO₂ concentration (at 50 cm depth) and surface flux

were measured. Soil CO₂ concentrations indicate a low background level (0.35±0.01%; Fig. 8). The distribution of CO₂ contents (Fig. 9) allows setting the threshold for anomalous soil CO₂ concentration at 0.5%, regardless of statistical method used (Sinclair 1974; Klusman 1993; Chiodini et al. 1998; Baubron et al. 2002). Between sites 9158715 and 9158990 (Fig. 8), soil CO₂ concentrations were frequently higher (up to twice) than the threshold value. Soil gases from selected sites were also analysed for He and Rn concentrations (Table 1). Helium indicates a significant anomaly which can only be explained by deep gas contamination (concentrations up to 5.282 ppm relative

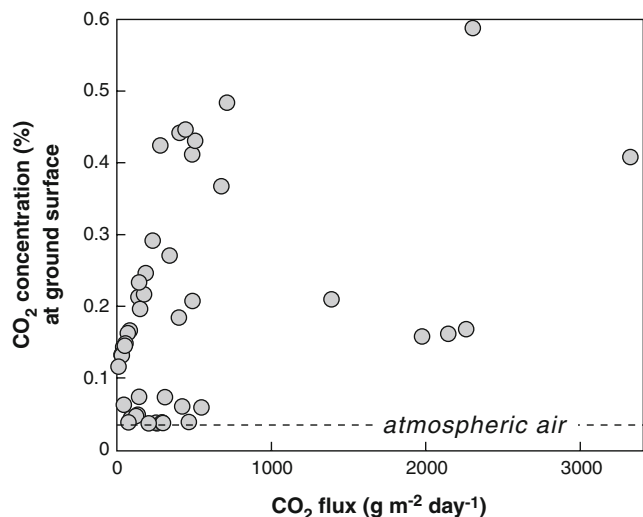


Fig. 7 Relationship observed at Merapi summit between CO₂ concentration emanating at ground surface and soil CO₂ flux

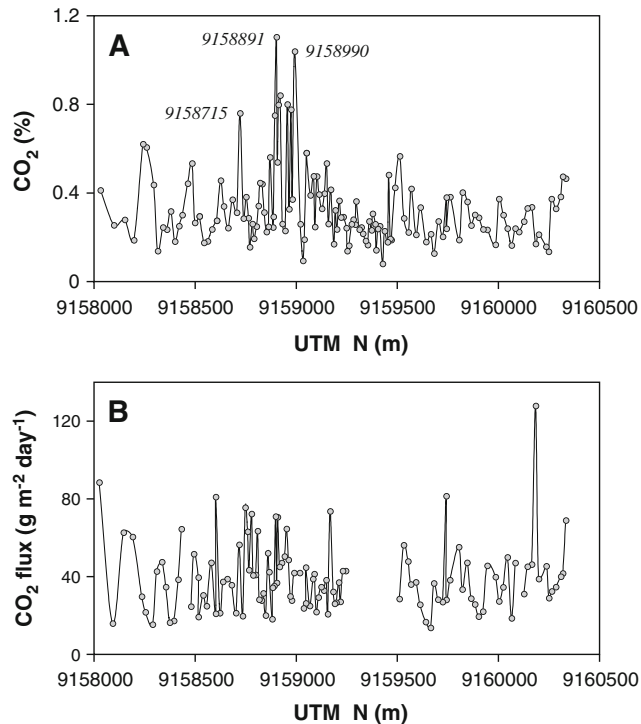


Fig. 8 a Soil CO₂ concentration values measured along the Waron traverse. Empty dots with numbers indicate sites suitable for a permanent monitoring of soil gases with radon automated probes. b Soil CO₂ flux for the Waron traverse

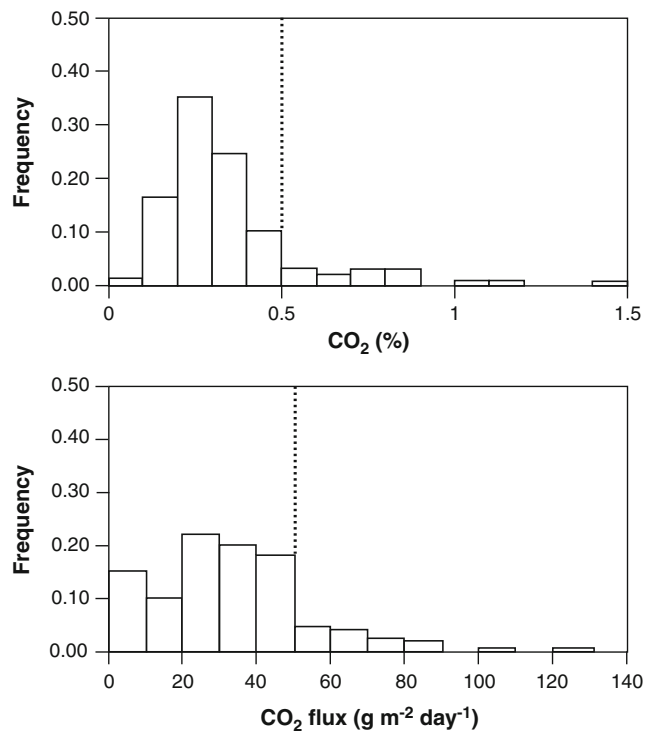


Fig. 9 Frequency distribution of soil air CO₂ concentration (a) and soil CO₂ flux values (b) measured along the Waron traverse. Vertical bars indicate anomaly thresholds

to atmospheric air (5.239 ppm), with a threshold value of 5.250 ppm). Radon concentrations were low (from about 1,000 to about 1,800 Bq m⁻³) and consistent with a generally low CO₂ flux that means the carrier gas is not flowing fast enough to avoid almost complete Rn decay before the gas reaches the surface. Nevertheless, He indicates the existence of a deep gas leakage, which would contribute to the slight increase in soil CO₂ concentration.

At Waron, the mean soil CO₂ flux is 37.8±1.4 g m⁻² day⁻¹, and the threshold above which flows can be considered as anomalous (due to either a higher biogenic activity or a deep gas exhaust) is 50 g m⁻² day⁻¹. However, field evidence (moist soils with particularly vegetation development) suggests that the highest flux values are related to biogenic activity.

Discussion

Merapi undergoes permanent volcanic activity, leading to high temperatures below the central edifice (Commer et al. 2006). Tropical rainfall leads to huge meteoric inflows through the young volcanic deposits at the surface. Multiformal fluid circulations and hydrothermal activity resulting from these features have been already outlined through conductivity and resistivity measurements (Muller and Haak 2004; Commer et al. 2006), self-potential

mapping (Aubert et al. 2000), self-potential continuous monitoring (Friedel et al. 2004) and geochemical characteristics of high-temperature fluids (Zimmer and Erzinger 2003). Commer et al. (2006) suggested from resistivity modelling the existence of both secondary minerals derived from hydrothermal alteration and hypersaline (~25 eq. wt.%) high-temperature fluids extending southerly and heated by ascending lava and/or gas–steam mixtures. Muller and Haak (2004) estimated the top of the saline fluid body to be 300 m below Merapi summit. These results strongly suggest the existence of a central hydrothermal system associated with magma-filled pockets or a magma chamber, operating at various depths and characterized by fluid transfer closely controlled by shallow structural heterogeneities.

Carbon dioxide mapping at the surface (Fig. 4) exemplifies the control on fluid transfer exerted by major volcano-tectonic structures. Carbon dioxide degassing likely originates from either direct magma exsolution or hydrothermal solution boiling, or both. Decreasing soil CO₂ concentrations with increasing distance from crater may suggest an inverse relationship between CO₂ concentration at surface and the distance the gas has to rise, i.e. the longer the route, the higher the dilution by air. Buried crater rims related to major historical eruptions (1768, 1872, 1930–1932, 1953) clearly act as boundaries confining concentric areas.

These crater rims may act either as a sealed barrier (with hydrothermal deposits) or as preferential channels for meteoric fluid inflow. Secondary mineral precipitation is a known process at active volcanoes, because the degassing vapour interacts with meteoric waters and promotes deposition of mineral sequences as a function of temperature, acidity and redox potential. Deposition upon cooling of clays, alunite, anhydrite, pyrite and silica were described by Giggenbach (1992). This scenario is compatible with the results of recent ground resistivity measurements (Commer

Table 1 Selected soil gas compositions at Waron traverse

X	Y	CO ₂	He ppm	Bq m ⁻³
9159900	438842	0.760	5.282	1,210
9159900	438845	0.883	5.284	1,380
9159901	438848	0.860	5.282	1,740
9159901	438853	0.511	5.255	907
9159900	438838	0.854	5.271	1,670
9158990	438863	1.506	5.296	1,705
9158990	438867	0.464	5.249	1,596
9158990	438858	0.778	5.238	1,160
9158719	438835	0.869	5.216	1,233

Sampling depth of 0.5 m. Uncertainties on concentrations are: CO₂: ±0.5%; He: ±0.002 ppm; ²²²Rn: ±10%. Displayed data are mean values of duplicate samples

et al. 2006), although Muller and Haak (2004) disagreed with this hypothesis. Secondary mineral precipitation is also suggested by density contrasts in the summit area deduced from gravimetric imaging (Gunawan 2005). Hydrothermal mineralization operates mainly along the main pathways that allow fluid transfers, such as the former crater rims, characterized by a drastic fall in permeability, making these rims sealed barriers. On the other hand, the crater rims may also undergo repeated downward meteoric flushing due to heavy rainfall. The two mechanisms may act together; the 1932 and 1872 (and maybe the 1769) crater rims acting as impervious surfaces for downward channelling of meteoric water. Figure 10 is a schematic SW–NE cross-section of Merapi which displays the main volcano-tectonic structures and the suggested upward and downward fluid motions.

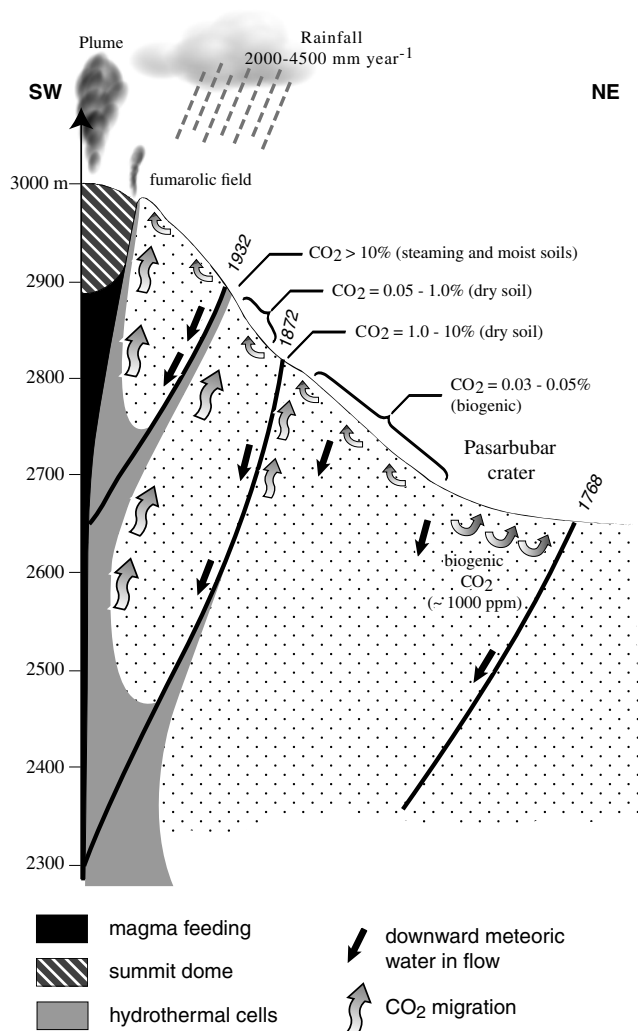


Fig. 10 Schematic cross-section of Merapi summit, showing a model of fluids circulation based on the geochemical data obtained from the present work. Also shown are the major volcano-tectonic structural discontinuities, interpreted as old caldera rims. Altitudes in metres above sea level

The scenario of CO₂ degassing in homogeneous confined areas is not valid for two restricted areas. Firstly, north of the 1932 crater rim, higher CO₂ concentrations (up to 10%) seem to delineate a N40°E directed degassing anomaly. This anomaly coincides with the 1953 crater rim described by Camus et al. (2000). This matches the area where large horizontal displacements are evidenced from kinematic GPS measurements and interpreted in terms of summit rigid blocks motion and active discontinuities, among which is a N20°E active fracture (Beauducel et al. 2006). This active structure is also coherent with the 2D Bouguer gravity anomaly map of the summit outlining separate blocks that match well the horizontal displacements.

Secondly, the northern rim of the 1904 crater, which is occupied by the Woro fumarolic field, displays extremely variable CO₂ concentrations within 10 meters. This suggests that both mineral sealing of the rim, leading to low CO₂ degassing, and continuous motion of rigid blocks, leading to new fracture generation and subsequent high permeability, allow CO₂ degassing to operate within a very restricted space. However, these exceptions to the overall picture of confined and homogeneous low degassing areas strengthen the hypothesis of a control of permeability and degassing features by the major tectonic framework which undergo either mineral sealing or fracturing.

Measurements of the crater SO₂ flux performed routinely at Merapi indicate a mean flux of 100 T day⁻¹ during quiescent periods. Assuming a mean CO₂/SO₂ molar ratio of 3.5 based on high temperature gas analyses, 240 T day⁻¹ of CO₂ are emitted by the degassing dome. The first estimate for the diffuse summit degassing of 200 to 230 T day⁻¹ for the non-erupting northern part of the volcano is about half of the total output of CO₂ and therefore must be considered when estimating the bulk volatile budget during inter-eruptive periods.

On the lower southern slope (Waron traverse), the location of the weak soil degassing anomaly fits quite well with the structural model from Kalscheuer et al. (2007). In detail, the anomaly is a small distance (about 250–300 m) to the south of the inferred structure. This suggests a down slope transfer of rising gases from the 450 to 900 m-deep hydrothermal source proposed by these authors by shallow underground water, although the observed shift may also indicate an irregular shape of the collapsed caldera rim.

Conclusions

Substantial amounts of CO₂ are released through soils from the flanks of Merapi summit. The estimated daily CO₂ output from the upper non eruptive northern flank of the volcano accounts for up to 50% of the total output during

quiescent periods. Soil gas surveys indicate that dilution of magmatic gases by massive inflow of atmospheric air into the slopes of the terminal cone makes soil CO₂ concentration low, even for relatively high gas flows. This is probably typical for summit soils of active volcanoes. The main structural features of the summit are associated with either CO₂ or soil temperature anomalies, fractures acting mainly as sealed barriers, whereas heat and gas transfer operate through isolated block junctions. This scheme is consistent with recent models based on resistivity, conductivity, self-potential, gravimetry and ground deformation studies.

A weak CO₂ and He degassing anomaly is located on the lower southern flank of the volcano and related to an expected deep hydrothermal reservoir connected to the surface by a major ancient avalanche caldera rim. This site has been equipped with a permanent monitoring station of ²²²Rn in soil air, radon being used as a tracer for gas flow.

Finally, diffuse degassing patterns help to constrain the structure of Merapi. Large fractures retain high enough permeability through time to allow permanent gas transfer even at distance from the magmatic fluid circulation system such as that linked to the ancient caldera rim. Conversely, fractures close to the dome are quickly sealed by secondary minerals, because they undergo severe mineral alteration due to their proximity to the magmatic fluid feeding system. Despite the small data set of soil CO₂ fluxes for the non-erupting portion of the summit cone, it suggests a significant contribution of diffuse degassing to the bulk CO₂ budget of Merapi volcano.

Acknowledgements This work was funded by the French Embassy in Jakarta (Indonesia) under the general Franco-Indonesian bilateral cooperation in volcanology. We thank the DVGHM (Directorate of Volcanology and Geological Hazard Mitigation, Bandung, Indonesia) for supporting the cooperation. The manuscript was greatly improved by constructive comments from S. Giammanco. A detailed and critical review by Deborah Bergfeld, whose advice is warmly acknowledged, allowed for a better display of data and its interpretation. Dave G. Jones (BGS, UK) and Pierre Delmelle (editor in charge) strongly improved the English and the organization of the paper. This is IPGP contribution no. 2385.

References

- Allard P, Carbonnelle J, Dajlevic D, Le Bronec J, Morel P, Robe M-C, Maurenas J-M, Faivre-Pierret R, Martin D, Sabroux J-C, Zettwoog P (1991) Eruptive and diffuse emissions of CO₂ from Mount Etna. *Nature* 351:387–391
- Allard P, Carbonelle J, Dajlevic D, Metrich N, Sabroux J-C (1995) The volatile source and magma degassing budget of Merapi volcano: evidence from high-temperature gas emissions and crystal melt inclusions. In *Merapi Int. Decade Volcano Workshop, UNESCO/Volcanological Survey of Indonesia, Yogyakarta*, 16–17
- Allard P, Hammouya G, Parello F (1998) Dégazage magmatique diffus à la Soufrière de Guadeloupe, Antilles. *C R Acad Sci* 327:315–318
- Aubert M, Dana IN, Gourgaud A (2000) Internal structure of the Merapi summit from self-potential measurements. *J Volcanol Geotherm Res* 100:337–343
- Bahar I (1984) Contribution à la connaissance du volcanisme indonésien: le Merapi (Centre Java), cadre structural, pétrologie, géochimie et implications volcanologiques. PhD thesis, University of Montpellier
- Baubron J-C (1996) Etna Laboratory Volcano. Contrat EV5V-CT92–0177. Prospection, caractérisation et variabilité temporelle d'émanations gazeuses diffuses à l'Etna (Sicile-Italie). *Années 1993 et 1994*. Open file report, BRGM/RP-38820-FR (www.brgm.fr)
- Baubron J-C, Allard P, Toutain J-P (1990) Diffuse volcanic emissions of carbon dioxide from Vulcano island (Italy). *Nature* 344:51–54
- Baubron J-C, Allard P, Sabroux J-C, Tedesco D, Toutain J-P (1991) Soil gas emanations as precursory indicators of volcanic eruptions. *J Geol Society London* 148:571–576
- Baubron J-C, Rigo A, Toutain J-P (2002) Soil gas profiles as a tool to characterize active tectonic areas: the Jaut pass example (Pyrénées, France). *Earth Planet Sci Lett* 196:69–81
- Baubron J-C, Hamm V, Pinault J-L (2004) Elaboration de la méthodologie de mesurage et d'interprétation de la concentration en radon dans les habitations situées dans l'emprise de travaux miniers souterrains. Open file report, BRGM/RP-53886-FR (www.brgm.fr)
- Baxter P, Baubron J-C, Coutinho R (1999) Health hazards and disaster potential of ground gas emissions at Furnas volcano, Sao Miguel, Azores. *J Volcanol Geoth Res* 92:95–106
- Beauducel F, Agung Nandaka M, Cornet F-H, Diament M (2006) Mechanical discontinuities monitoring at Merapi volcano using kinematic GPS. *J Volcanol Geoth Res* 150:300–312
- Berthommier P (1990) Etude volcanologique du Merapi (Centre Java). Téphrostratigraphie et chronologie. Mécanismes éruptifs. PhD thesis, University Blaise Pascal, Clermont-Ferrand
- Camus G, Gourgaud A, Mossand-Berthommier P-C, Vincent P-M (2000) Merapi (Central Java, Indonesia): An outline of the structural and magmatological evolution, with a special emphasis to the major pyroclastic events. *J Volcanol Geoth Res* 100:139–163
- Chiodini G, Cioni R, Guidi M, Raco B (1998) Soil CO₂ flux measurements in volcanic and geothermal areas. *Applied Geochem* 13:543–552
- Chiodini G, Cardellini C, Frondini F, Granieri D, Marini L, Ventura G (2001) CO₂ degassing and energy release at Solfatara Volcano, Campi Flegrei, Italy. *J Geophys Res* 106:16213–16221
- Chiodini G, Granieri D, Avino R, Caliro S, Costa A, Werner C (2005) Carbon dioxide diffuse degassing and estimation of heat release from volcanic and hydrothermal systems. *J Geophys Res* 110: B08204, doi:10.1029/2004JB003542
- Commer M, Helwig SL, Hordt A, Scholl C, Tezkan B (2006) New results on the resistivity structure of Merapi Volcano (Indonesia), derived from three-dimensional restricted inversion of long-offset transient electromagnetic data. *Geophys J Int* 167:1172–1187
- D'Alessandro W, Parello F (1997) Soil gas prospection of He, ²²²Rn and CO₂: Vulcano Porto area, Aeolian Islands, Italy. *Applied Geochem* 12:213–224
- Farrar CD, Sorrey ML, Evans WC, Howles JF, Kerr BD, Kennedy BM, King CY, Southon JR (1995) Forest-killing diffuse CO₂ emission at Mammoth Mountain as a sign of magmatic unrest. *Nature* 376:675–678
- Friedel S, Byrdina S, Jacobs F, Zimmer M (2004) Self-potential and ground temperature at Merapi volcano prior to its crisis in the rainy season of 2000–2001. *J Volcanol Geotherm Res* 134:149–168
- Giammanco S, Inguaggiato S, Valenza M (1998) Soil and fumarole gases of Mount Etna: geochemistry and relations with volcanic activity. *J Volcanol Geotherm Res* 81:297–310

- Giggenbach WF (1992) Magma degassing and mineral deposition in hydrothermal systems along convergent plate boundaries. *Economic Geol* 87:1927–1944
- Gunawan H (2005) Gravimétrie et microgravimétrie appliquées à la volcanologie: exemples de la Soufrière de Guadeloupe et du Mérapi. PhD thesis, Institut de Physique du Globe de Paris
- Hernandez PA, Salazar JM, Shimoike Y, Mori T, Notsu K, Perez N (2001) Diffuse emission of CO₂ from Miyakejima volcano, Japan. *Chem Geol* 177:175–185
- Kalscheuer KM, Commer SL, Helwig A, Hördt A, Tezkan B (2007) Electromagnetic evidence for an ancient avalanche caldera rim on the south flank of Mount Merapi, Indonesia. *J Volcanol Geotherm Res* 162:81–97
- Klusman RW (1993) Soil gas and related methods for natural resource exploration. Wiley, Chichester
- Le Cloarec M-F, Gauthier P-J (2003) Merapi Volcano, Central Java, Indonesia: A case study of radionuclide behavior in volcanic gases and its implications for magma dynamics at andesitic volcanoes. *J Geophys Res* 108(B5), doi:10.1029/2001JB001709
- Lewicki JL, Connor C, St-Amand K, Stix J, Spinner W (2003) Self-potential, soil CO₂ flux, and temperature on Masaya volcano, Nicaragua. *Geophys Res Lett* 30(15):1817, doi:10.1029/2003GL017731
- Müller A, Haak V (2004) 3-D modeling of the deep electrical conductivity of Merapi volcano (Central Java): integrating magnetotellurics, induction vectors and the effects of steep topography. *J Volcanol Geotherm Res* 138:205–222
- Nho EY, Le Cloarec M-F, Ardouin B, Tjetjep WS (1996) Source strength assessment of volcanic trace elements emitted from the Indonesian arc. *J Volcanol Geotherm Res* 74:121–129
- Pinault J-L, Baubron J-C (1996) Signal processing of soil gas radon, atmospheric pressure, and soil temperature data: a new approach for radon concentration modeling. *J Geophys Res* 101:3157–3171
- Ratdomopurbo A (1995) Etude sismologique du volcan Merapi et formation du dôme de 1994. PhD Thesis, University Joseph Fourier, Grenoble
- Richter G, Wassermann J, Zimmer M, Ohrnberger M (2004) Correlation of seismic activity and fumarole temperature at the Mt. Merapi volcano (Indonesia) in 2000. *J Volcanol Geotherm Res* 135:331–342
- Salazar JML, Hernández PA, Pérez NM, Melián G, Alvarez J, Segura F, Notsu K (2001) Diffuse emission of carbon dioxide from Cerro Negro volcano, Nicaragua, Central America. *Geophys Res Lett* 28(22):4275–4278, doi:10.1029/2001GL013709
- Sinclair AJ (1974) Selection of threshold values in geochemical data using probability graphs. *J Geochem Explor* 3:129–149
- Sortino F, Nonell A, Toutain J-P, Munoz M, Valladon M, Volpicelli G (2006) A new method for sampling fumarolic gases: Analysis of major, minor and metallic trace elements with ammonia solutions. *J Volcanol Geot Res* 158:244–256
- Symonds RB, Rose WI, Reed MH, Lichte FE, Finnegan DL (1987) Volatilization, transport and sublimation of metallic and non-metallic elements in high temperature gases at Merapi Volcano, Indonesia. *Geochim Cosmochim Acta* 51:2083–2101
- Toutain J-P, Baubron J-C (1999) Gas geochemistry and seismotectonics: a review. *Tectonophysics* 304:1–27
- Toutain J-P, Baubron J-C, Francois L (2002) Runoff control of soil degassing at an active volcano. The case of Piton de la Fournaise, Reunion Island. *Earth Planet Sci Lett* 197:83–94
- Van Bemmelen RW (1949) The Geology of Indonesia, 1A. Martinus Nijhoff, The Hague
- Voight B, Constantine EK, Siswoidjyo S, Torley R (2000) Historical eruptions of Merapi Volcano, Central Java, Indonesia, 1768–1998. *J Volcanol Geotherm Res* 100:69–138
- Welles JM, Demetriades-Shah TH, McDermitt DK (2001) Considerations for measuring ground CO₂ effluxes with chambers. *Chem Geol* 177:3–13
- Williams-Jones G, Stix J, Heiligmann M, Charland A, Sherwood Lollar B, Garzón V, Barquero J, Fernandez E (2000) A model of diffuse degassing at three subduction-related volcanoes. *Bull Volcanol* 62:130–142
- Young KD, Voight B, Subandriyo, Sajiman, Miswanto, Casadevall TJ (2005) Ground deformation at Merapi Volcano, Java, Indonesia: distance changes, June 1988–October 1995. *J Volcanol Geotherm Res* 141:157–175
- Zimmer M, Erzinger J (2003) Continuous H₂O, CO₂, ²²²Rn and temperature measurements on Merapi Volcano, Indonesia. *J Volcanol Geotherm Res* 125:25–38